International Journal of Applied Earth Observation and Geoinformation 153 (2026) 105570

Contents lists available at ScienceDirect

International Journal of Applied Earth Observation and Geoinformation

journal homepage: www.elsevier.com/locate/jag

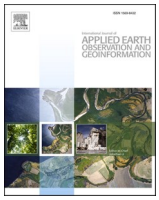

Monitoring forest growth dynamics from harmonized multi-source time series of canopy height

Hugo de Lame [a,b,*], Thibauld Collet [a], Pauline Depoortere [a], Alexia Favaro [a,c], Philippe Lejeune [a], Adrien Michez [a], Antoine Plumacker [a], Jérôme Perin [a], Thomas Pollet [a,d], Quentin Ponette [d], Zoé Rousseau [a], Arthur Vander Linden [a], Marie-Pierre Tasseroul [a], Christian Messier [b], Jean-François Bastin [a]

[a] University of Liège –TERRA Teaching and Research Centre, Gembloux Agro-Bio Tech. Passage des Déportés, 2, 5030 Gembloux, Belgium
[b] Département des sciences naturelles, Institut des sciences de la Forêt Tempérée (ISFORT), Université du Québec en Outaouais (UQO), Ripon, QC J0V 1V0, Canada
[c] Forest & Nature Lab, Ghent University, Geraardsbergsesteenweg 267, 9090, Belgium
[d] UCLouvain, Earth & Life Institute, Croix du Sud 2, 1348 Louvain-la-Neuve, Belgium

A B S T R A C T

Most remote sensing assessments of forest change focus on canopy cover, whereas the dynamics of vertical growth remain less investigated despite their sensitivity to external forcings. Yet, the increasing availability of canopy height products from multiple platforms facilitates spatially explicit characterization of vertical growth dynamics, provided that systematic measurement biases between sources are properly addressed. Here, we present a transferable workflow to map vertical growth dynamics from mixed-source canopy height model (CHM) time series, harmonized against forest inventory plots at ~ 1000 m^2 resolution. We estimated vertical growth to model reference trajectories as a function of initial canopy height. Deviations from these trajectories were quantified, providing contextualized growth information. This approach was illustrated in the Belgian Ardenne using multi-source CHMs derived from recent aerial imagery and lidar data (2006–2021). Across all acquisitions, harmonization reduced systematic bias in dominant height estimates from 2.53 m to 0.01 m (RMSE = 1.79 m, R2 = 0.92), with canopy structure rather than acquisition parameters as the primary driver of bias. Subsequent growth decreased as initial heights increased, with earlier declines in broadleaf than coniferous stands. Spatially clustered growth deviations (Moran's I = 0.31–0.46, $p < 0.001$) suggested systematic variation in performance among otherwise similar forests. By leveraging heterogeneous sources of canopy height, this workflow enables spatially exhaustive characterization of forest growth, adding structural understanding into multi-scale forest monitoring and resilience assessments.

1. Introduction

To monitor the dynamics of forest ecosystems, traditional ground-based inventories provide recurrent high-quality measurements of plot-level forest attributes, mainly basal area and top-height (Rondeux, 2021), but risk missing non-recurring or localized information as operational costs constrain their spatial and temporal coverages. On the other hand, remote sensing provides spatially explicit information at lower costs (Wulder et al., 2008; Coops, 2015), but forest change is mostly quantified through canopy cover derived from surface reflectance (Hansen et al., 2013; Senf and Seidl, 2021), with densifying time series now allowing continuous monitoring rather than discrete detection (Woodcock et al., 2020). While cover-based approaches effectively quantify horizontal expansion, they ignore vertical variations at the risk of overestimating, for example, post-disturbance recovery when structural attributes other than cover remain altered (Feng et al., 2021; Runge et al., 2025).

Yet, vertical dynamics mirror key demographic processes of growth, mortality and recruitment. Vertical growth especially reflects ecosystem productivity and modulates biomass accumulation, structural complexity, and resilience to disturbances (Ehbrecht et al., 2021; Falk et al., 2022); its spatial patterns capture trade-offs among productivity, microclimate buffering, and biodiversity distribution, making it a crucial indicator of forest functioning (Yu et al., 2008). Forests develop differently depending on their composition, structure, and functional strategies, in a mosaic of patches continually rearranging in response to climate change, disturbances or management (Pretzsch, 2020). Despite their ecological significance, spatial patterns of vertical growth remain insufficiently characterized beyond the stand level. This limits our ability to capture subtle trends and detect unusual deviations from expected trajectories, all of which are valuable for attributing changes to specific drivers (Seidl et al., 2017; Fassnacht et al., 2025) and improving

* Corresponding author.
E-mail address: hugo.delame@uliege.be (H. de Lame).

https://doi.org/10.1016/j.jag.2026.105570
Received 3 April 2026; Received in revised form 3 September 2026; Accepted 3 September 2026

forecasts under shifting environmental conditions (Pretzsch et al., 2014). Such challenges are particularly relevant in northern temperate forests where structural homogeneity from past management increased vulnerability (Gilles et al., 2024).

In these regions, spatially and temporally explicit assessments of vertical growth require consecutive measurements of the same forest's canopy height to be reliable (Hyyppä et al., 2003; McRoberts et al., 2015). Among canopy attributes, dominant height measures the uppermost canopy layer made of the dominant and co-dominant trees driving stand-level processes, and is commonly used for growth monitoring given its continuous variation over time and close tie with productivity. In practice, stand-level dominant height is measured in the field using the mean height of the largest trees (Rondeux, 2021); remote sensing surveys estimate it using top-of-canopy height (TCH), typically a high percentile of measurements which remains consistent across data sources and closely matches its field-based counterpart (St-Onge et al., 2008; Hopkinson et al., 2008). TCH is mostly retrieved by lidar through airborne laser scanning (ALS; Hyyppä et al., 2003; Zhang et al., 2025), with most European territories now covered at least once, although few have been resurveyed since their first acquisition (Moudrý et al., 2026); spaceborne platforms are beginning to offer complementary canopy height estimations with a near-global coverage (Markus et al., 2017; Schlund et al., 2019; Dubayah et al., 2020), but remain limited by their short temporal span and by variable accuracy over complex canopies. Few regions therefore have enough consecutive, spatially explicit canopy height assessments to enable regional monitoring of vertical growth, particularly for earlier periods.

A solution to this limited temporal coverage lies in digital aerial photogrammetry (DAP), which reconstructs canopy surfaces from overlapping images acquired by airborne or, increasingly, drone-based cameras (Goodbody et al., 2017). Although image-based DAP only captures the upper canopy layer, associating it with ALS unveils longer-term patterns of dominant height changes, otherwise inaccessible with a single acquisition (Goodbody et al., 2019). Digital surface models (DSM) produced by DAP are normalized into canopy height models (CHM) using an ALS-based digital terrain model (DTM). Whereas lidar acquisitions are generally performed during leaf-off conditions, DAP benefits from leaf-on for accurate canopy reconstruction (Michez et al., 2020). DAP also permits higher surveying altitudes at lower costs, while archived orthoimages extend time series backwards beyond ALS availability (Price et al., 2020).

Despite this demonstrated potential, combining DAP and ALS products into usable, multi-source time series requires accounting for systematic biases between acquisitions, caused by factors varying from acquisition conditions to canopy structure differences (Næsset, 2002; Wu et al., 2020; Mielcarek et al., 2020). Biases propagate uncertainty into vertical growth estimation, especially over short periods. Harmonizing bias is thus essential to ensure genuine reflection of vertical growth rather than acquisition artifacts, particularly with heterogeneous sources of canopy height. Previous small-scale growth studies aligned successive point clouds using permanent features from a reference ALS acquisition, or canopy heights updated from growth models (Riofrío et al., 2022; Janiec et al., 2024). At larger scales, albeit not targeting forest dynamics, acquisition-related predictors were used to model measurement bias between yearly DAP and field inventories (Michez et al., 2020), similarly to area-based approaches calibrating wall-to-wall datasets from sparse plots (Bolton et al., 2018), since such references offer quality-controlled measurements of dominant height across diverse conditions (Tomppo et al., 2010). Still, this preprocessing has not yet been systematically adopted for heterogeneous canopy height time series, with no consensus on methodology nor quantification of its impact.

In this context, we developed a workflow to exhaustively quantify spatial patterns of vertical growth in forested landscapes using harmonized multi-source (ALS and DAP) time series of dominant height, transferable to forested regions where multiple acquisitions and field inventory are available. We addressed the following research questions: (1) Can harmonized multi-source time series of dominant height capture realistic patterns of vertical growth? And (2) do deviations from reference trajectories reveal spatial contrasts in forest performance? We illustrated and validated this approach in Belgian temperate forests over 2006–2021.

2. Materials and methods

We applied our workflow in Belgium's Ardenne (Fig. 1). To prevent between-source systematic bias from propagating into wall-to-wall time series of TCH-estimated dominant height, we developed a harmonization model aligning multi-source canopy height acquisitions from 2006 to 2021 against field-measured dominant height from single-visit inventory plots. We then applied this model to generate consistent time series, both at landscape-scale where we derived spatially explicit vertical growth trends across hexagonal grid cells (~1000 m^2), and at representative plots randomly sampled across the region to model species-specific reference trajectories by space-for-time substitution. Cell-level deviations against these references provided contextualized assessments of vertical growth.

2.1. Study area

The Ardenne (Fig. 2) spans 5630 km^2 in southern Belgium, with forests covering 58% of the area from ~ 350 to ~ 700 m above sea level

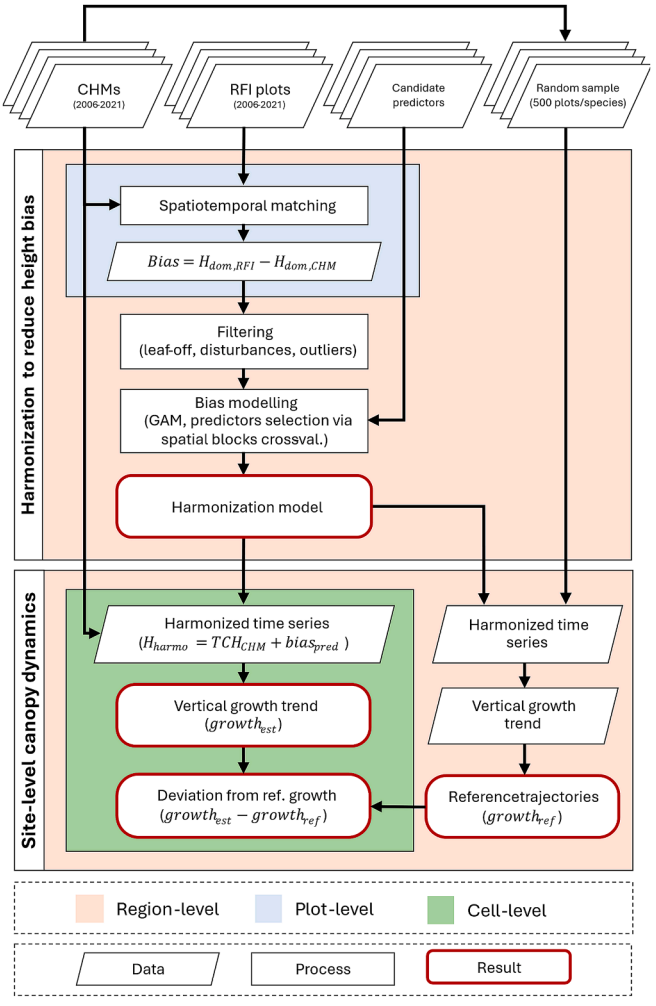

Fig. 1. Methodological workflow. Only significant processes are explicitly labeled.

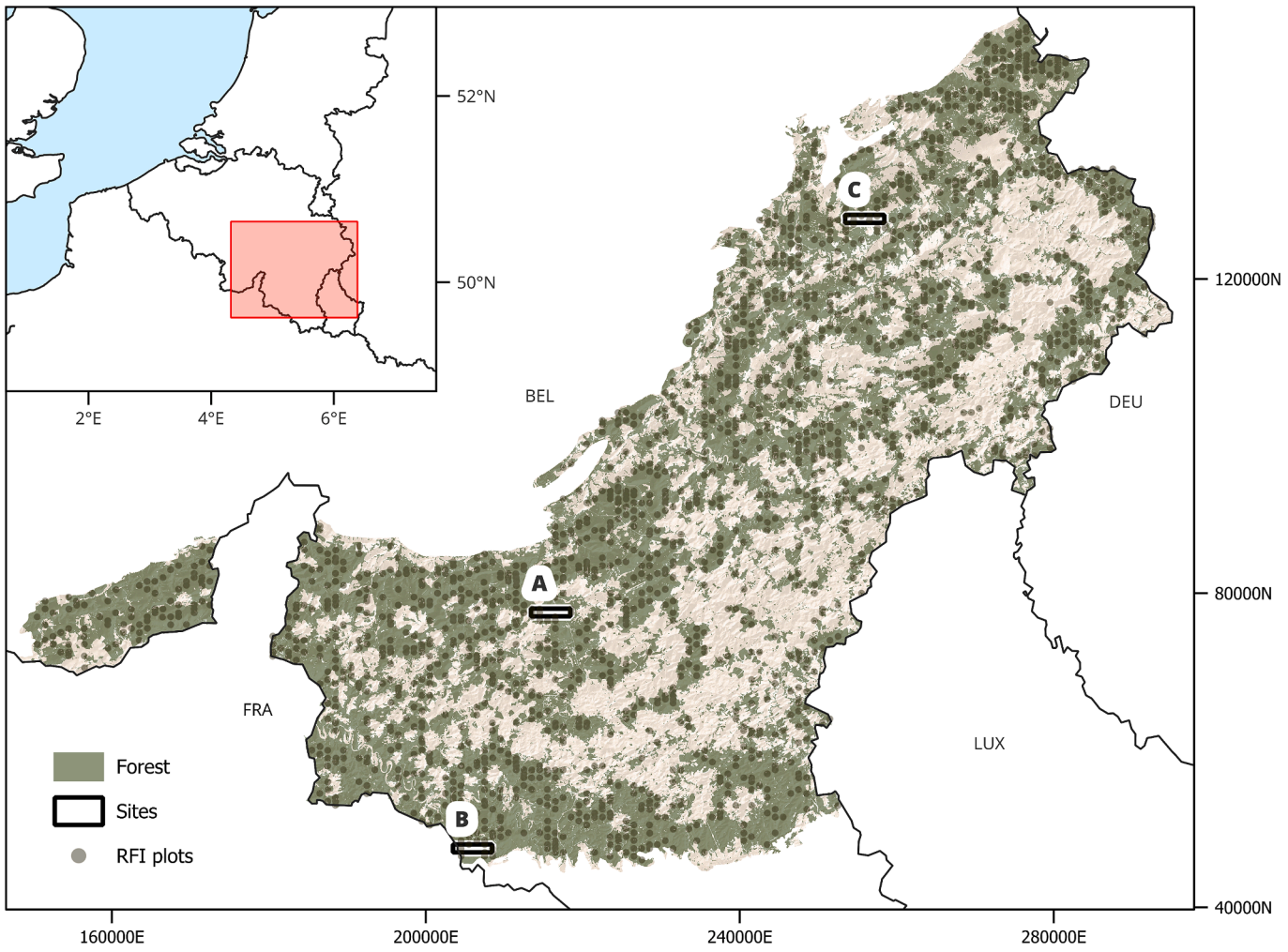

Fig. 2. Study area in the Ardenne region, southern Belgium. Dots indicate the reference field plots from the Regional Forest Inventory (RFI). Yellow circles mark the location of the case study sites. (For interpretation of the references to colour in this figure legend, the reader is referred to the web version of this article.)

on the south-west to north-east axis. Mean annual temperatures decrease along this gradient from 10°C to 7.5°C, while total precipitation ranges from 1000 to 1400 mm. Combined with topography alternating between slopes, plateaus and valleys, these variations create different microclimatic conditions.

Forest composition, under heavy anthropogenic influence, is representative of European temperate forests. Broadleaf stands (43%) are dominated by beech (*Fagus sylvatica* L.) and oak (*Quercus robur* L. & Quercus petraea (Matt.) Liebl), with birch (Betula spp.) and poplar (Populus × euramericana Guinier) in lesser proportions. Coniferous stands (57%) are largely composed of Norway spruce (*Picea abies* (L.) H. Karst), with Douglas-fir (*Pseudotsuga menziesii* (Mirb.) Franco), larch (Larix spp.), and pine (Pinus spp.) also present. Coniferous stands are mostly managed as even-aged plantations, with more homogeneous canopies compared to broadleaves (Alderweireld et al., 2015).

We selected three contrasting 5 × 1 km^2 case study sites (A, B, C; Fig. 2) to map growth patterns. Site A occupies well-drained plateaus with broadleaf dominance; Site B features mixed composition along south-facing valley slopes; and Site C is predominantly coniferous with heterogeneous terrain including seasonally waterlogged soils (Tossens et al., 2024). All sites contained beech, our focal species for cross-site comparison given its wide ecological plasticity and sensitivity to climate change (Martinez del Castillo et al., 2022).

2.2. Data sources

2.2.1. Canopy height models (CHMs)

CHMs represented canopy height for a single year, derived from region-wide official DAP or lidar acquisitions performed at irregular intervals between 2006 and 2021, each generated at its native GSD from multiple flights conducted over the corresponding surveying period (Table 1). Lidar CHMs were derived from ALS surveys conducted mostly

Table 1
Characteristics of the aerial surveys used to derive CHM time series in the Ardenne.

Survey reference	Source	GSD (m)	Acquisition period
2006	DAP	1	June 2006–April 2007
2009	DAP	0.5	May 2009–July 2010
2012	DAP	0.5	May 2012–July 2013
2014	lidar	0.5	December 2012–March 2014
2015	DAP	0.5	April 2015
2016	DAP	0.5	June 2016–November 2016
2018	DAP	0.5	May 2018–June 2018
2019	DAP	0.5	June 2019–August 2019
2020	DAP	0.5	April 2020
2021	lidar	0.5	February 2021–March 2022

during the leaf-off period for the years 2014 and 2021. Photogrammetric CHMs were generated following Michez et al. (2020) by differentiating leaf-on image-based DSMs, acquired triennially from 2006 and then annually from 2015 (except 2017), against the 2014 ALS-based DTM. We excluded broadleaf pixels surveyed under leaf-off conditions, whether by DAP or by lidar in spring 2013, to avoid reconstruction artifacts.

2.2.2. Regional forest inventory (RFI) plots

The RFI uses a systematic sampling design distributed throughout the Ardenne (Perin, 2023; Fig. 2), as in national forest inventories. The circular plots have an 18 m radius (1018 m^2) where numerous attributes are measured, including species identification and tree height using dendrometers (Alderweireld et al., 2015). Notably, no RFI plot was revisited during the study period, meaning each plot provides a single temporal observation.

Each RFI plot was paired with all CHM acquisitions performed within one year of their field inventory date, so that height differences reflected systematic measurement bias rather than natural growth (Price et al., 2020); a single RFI plot could therefore match multiple CHM years. Plot centers were then located on the CHMs using co-registered GNSS positions to correct potential positioning errors, and pixel values extracted within the plot radius, which further mitigated potential residual spatial offsets.

2.2.3. Ancillary maps

To determine the dominant tree species and broadleaf-to-conifer ratio, we used additional reference rasters (Bolyn et al., 2022; Lejeune et al., 2025) rather than RFI data, as these maps enabled region-wide extrapolation. The composition map includes 10 classes: beech, birch, Douglas-fir, larch, oak, poplar, pine, and spruce, plus two residual classes for other broadleaf and coniferous species. Poplars were merged into other broadleaves, as only 8 RFI plots were poplar-dominated. We excluded all plots located outside forests on the composition map because of land use change since their installation.

2.3. Harmonizing systematic bias in aerial dominant height measurements for wall-to-wall time-series generation

The bias between field-measured dominant height and its CHM-based estimate could only be observed at sparse RFI plot locations (Eq. (1). While TCH is the best single proxy for dominant height, a systematic offset remains, known to vary with acquisition- and plot-related features (Næsset, 2002; Mielcarek et al., 2020). To enable further wall-to-wall extrapolation into harmonized, consistent time series of dominant height, we therefore modeled this systematic bias as a function of said features provided wall-to-wall availability.

2.3.1. Systematic bias preprocessing and filtering

For each RFI plot–CHM pair, we measured the systematic bias of dominant height as:

$$Bias = H_{dom,RFI} - H_{dom,CHM} \quad (1)$$

where $H_{dom,RFI}$ is the dominant height, and $H_{dom,CHM}$ is the best single proxy for estimating dominant height, the top-of-canopy height (TCH). Following RFI standard protocol of using the $(plot_{area}/10) - 1$ largest trees for plots below 5000 m^2 (Rondeux, 2021), we accordingly defined $H_{dom,RFI}$ as the mean height of the 9 largest-diameter trees within the 1018 m^2 inventory plots. TCH was chosen for $H_{dom,CHM}$ as it best minimized the difference with field-measured dominant height (St-Onge et al., 2008; Hopkinson et al., 2008); following sensitivity analysis (see Appendix S1), we defined TCH as the 95th percentile of canopy height pixels (0.5–1 m resolution; Table 1) within the plot boundary, which also limited artifacts caused by measurement outliers.

We excluded RFI plots whose dominant height dropped by more than 50% and 5 m at the later survey date, indicating disturbance during the interval (Senf and Seidl, 2021; Mielcarek et al., 2020), and removed outliers following Tukey's rule (bias exceeding 1.5 × IQR), which mainly excluded broadleaf plots from 2015 and 2020. Our final dataset contained 2,554 plot–CHM pairs distributed across the Ardenne for 2006–2021 (Table 2).

2.3.2. Candidate predictor variables

We selected candidate predictors of systematic bias based on previous CHM studies (Mielcarek et al., 2020; Michez et al., 2020), restricted to variables available wall-to-wall to ensure further extrapolation (Table 3).

2.3.3. Harmonization model fitting and selection

We fitted a generalized additive model (GAM) against our candidate predictors (Table 3) to predict the systematic bias in TCH-based dominant height estimation, enabling wall-to-wall extrapolation across CHMs into consistent time series of dominant height. We used a penalized thin-plate spline GAM fitted by REML (*mgcv*; Wood, 2000), which reduces errors for shorter canopies relative to linear models, as shown by Leclère et al. (2024) in the same region:

$$Bias = \beta_0 + \sum_j \beta_j x_{ij} + \sum_k f_k(z_{ik}) + \varepsilon_i \quad (2)$$

where i indexes the observations (RFI plot–CHM pairs), β_0 is the intercept, x_{ij} are categorical covariates with associated linear coefficients β_j, $f_k(\cdot)$ are penalized thin-plate spline smooth functions applied to continuous predictors z_{ik}, and $\varepsilon_i \sim N(0, \sigma^2)$ is the residual error.

We tuned the model through RMSE-based stepwise selection of candidate predictors (0.01 m threshold). Each step involved a 10-fold spatial cross-validation repeated 5 times, with spatial block size of 16,636 m estimated via variogram analysis using *blockCV* (Valavi et al., 2019). Once RMSE stabilized, the final model was fit to the full dataset to compute predicted bias, which was then added to TCH to generate harmonized dominant height estimates. All reported harmonization metrics (bias, RMSE, R^2) were computed from cross-validation holdouts.

We developed two model versions, with and without temporal variables, because the inclusion of temporal variables would constrain extrapolation by requiring temporally matched flight metadata and field data for new acquisitions.

2.4. Spatially explicit patterns of canopy height dynamics

We mapped canopy height dynamics onto the three study sites (Fig. 2), subdivided into hexagonal grid cells (~1000 m^2) approximating circular RFI plots used for bias harmonization. We extracted time series of dominant height (harmonized and original TCH) from all available acquisitions (Table 1), simultaneously within grid cells for spatially explicit landscape-scale mapping, and at randomly sampled forest plots for modeling of species-specific reference trajectories. We calculated growth trends at both levels based on these time series, then derived cell-level deviations from the reference trajectories.

2.4.1. Time series preprocessing and filtering

We considered a time series disturbed when TCH suddenly dropped by more than 50% (minimum 10 m drop) without recovering to 66% of pre-drop height within the two subsequent acquisitions, distinguishing genuine disturbances from artifacts or measurement noise. We similarly removed artifacts, defined as abrupt TCH gains or losses that were neither sustained across the series nor corrected by harmonization: a TCH value was flagged when it deviated by more than 50% from the median of adjacent acquisitions ($t \pm 1$) and more than 30% from broader neighbors ($t \pm 2$), with a minimum 2 m difference from the following acquisition.

Table 2
Plots distribution by reference acquisition year and dominant species class. Sample sizes reflect the regional species distribution.

Reference year	Dominant species									
	Beech	Birch	Douglas-fir	Larch	Oak	Oth. brdlf	Oth. cnfrs	Pine	Spruce	**Total**
2006	10	13	5	2	7	1	3	4	48	**93**
2009	29	17	12	3	25	8	5	12	90	**201**
2012	23	10	25	10	35	8	9	15	115	**250**
2014	20	11	36	9	26	6	21	9	144	**282**
2015	3	14	64	19	8	3	40	15	215	**381**
2016	53	18	54	16	72	11	32	20	209	**485**
2018	11	7	30	7	19	6	20	14	129	**243**
2019	25	8	34	10	28	5	23	13	136	**282**
2020	13	7	20	5	11	3	19	10	135	**223**
2021	12	2	13	5	19	3	16	5	39	**114**
Total	**199**	**107**	**293**	**86**	**250**	**54**	**188**	**117**	**1260**	**2554**

Table 3
Candidate predictors used to harmonize the measurement bias. Temporal, source, and canopy structure variables vary by CHM acquisition whereas forest composition and site conditions are derived from time-invariant ancillary maps.

Parameter	Explanatory variable	Category	Nature
Julian day	Day of year (1–365)	Temporal	Quantitative
Month	Month of acquisition (1–12)	Temporal	Quantitative
Season	Season of acquisition	Temporal	Quantitative
Acquisition year	Year of aerial survey	Temporal	Qualitative
CHM source	Lidar or DAP	Source	Qualitative
Top-of-canopy height (TCH)	95th percentile of canopy height within plot (m)	Canopy structure	Quantitative
Mean canopy height	Mean canopy height within plot (m)	Canopy structure	Quantitative
Canopy heterogeneity	Standard deviation of canopy height (m)	Canopy structure	Quantitative
Gap fraction	Proportion of pixels below 50% of TCH	Canopy structure	Quantitative
Dominant tree species	Dominant tree species	Forest composition	Qualitative
Broadleaf-conifer ratio	Ratio of broadleaves to conifers	Forest composition	Quantitative
Altitude	Mean elevation within plot (m)	Site conditions	Quantitative
Slope	Mean local slope within plot (m)	Site conditions	Quantitative
Topographic position	Plateau, valley or slope	Site conditions	Qualitative

2.4.2. Vertical growth trend

As 15 years remains relatively short from a stand development perspective, we deliberately approximated dominant height change as a simple linear indicator of both magnitude and direction, interpretable and spatializable across levels, rather than a precise measure of productivity. At both sample plots and site-level grid cells, we therefore quantified vertical growth trend from the CHM time series as the slope of an ordinary least squares (OLS) regression of TCH over time:

$$TCH_{i,t} = \beta_{0,i} + \beta_{1,i} * t + \varepsilon_{i,t} \quad (3)$$

where for cell (or plot) i, t is the time, $\beta_{0,i}$ is the intercept, $\beta_{1,i}$ is the slope (our vertical growth trend indicator) and $\varepsilon_{i,t}$ the residual error term.

2.4.3. Species-specific reference trajectories of vertical growth

We established reference trajectories of vertical growth through space-for-time substitution, with initial TCH variations as a proxy for successive developmental stages along the trajectories. We drew 500 random samples (18 m radius, ~1000 m^2) per species, restricted to undisturbed plots with initial TCH > 2 m pre-harmonization in 2006 to avoid measurement uncertainty at low heights and early establishment effects from plantation lag, browsing, and seedling recruitment (Oliver and Larson, 1996). Bootstrapping (1000 iterations) confirmed stable slope estimates across species (SE = 0.0005–0.0015 m/yr; 95% CI width < 0.006 m/yr).

As canopy height typically follows a sigmoidal growth trajectory with asymptotic decline at maturity (Weiskittel et al., 2011; Pretzsch, 2020), and considering that we captured plots beyond the inflection point given our initial TCH threshold, we then modeled species-specific reference growth trajectories as an exponential decay of vertical growth toward a null asymptote against initial TCH in 2006; for each species s, we fitted separate nonlinear least squares (NLS) regressions for non-harmonized and harmonized trends:

$$\beta_{1,i} = K_{a,s} * (K_{b,s})^{TCH_{i,2006}} + \delta_i \quad (4)$$

where $\beta_{1,i}$ is the growth trend computed from Eq. (3) at sample plot i, $TCH_{i,2006}$ is the TCH at the start of the time series (2006), $K_{a,s}$ is the species-specific growth rate at minimal initial height, $K_{b,s}$ the species-specific decay coefficient, and δ_i the plot-level residual.

2.4.4. Deviation from reference growth

Finally, cell-level deviation was the residual from the reference trajectory, by rearranging Eq. (4):

$$\delta_i = \beta_{1,i} - (K_{a,s} * (K_{b,s})^{TCH_{i,2006}}) \quad (5)$$

where positive δ_i indicate plots growing faster than expected for their species and initial canopy height; negative values indicate underperformance compared to the regional reference.

2.4.5. Propagation of harmonization uncertainty

We propagated harmonization uncertainty into deviations through Monte Carlo simulation. For each plot–CHM pair, dominant height uncertainty was estimated as the standard deviation of harmonized TCH in cross-validation folds, and propagated 1000 times through growth trends (Eq. (3) and initial 2006 heights, both fed into the reference trajectories (Eq. (4) for refitting before re-computation of deviations.

2.4.6. Spatial patterns of growth

We applied the harmonization model without temporal variables to 5 × 1 km2 windows across our three case study sites (Fig. 2), then tested for spatial autocorrelation of cell-level growth trends and deviations using Moran's I. Spatial weights were constructed from an 8-nearest neighbors graph based on hexagonal cell centroids with row-standardized weights, using the *spdep* R package (Bivand et al., 2013).

3. Results

3.1. Harmonization to reduce height bias

For both models, stepwise selection retained in that order of importance: broadleaf-to-conifer ratio, gap fraction, and canopy height heterogeneity as smooth terms, all three highly significant with near-identical partial effects regardless of temporal variables inclusion

(Fig. S2). As for parametric coefficients, the temporal model attributed distinctly larger bias for the two lidar acquisitions of 2014 and 2021 (−1.47 and − 1.77 m; t = − 6.62 and − 6.93, both $p < 0.001$) than their DAP-counterparts (−0.12 to − 0.92 m; t from − 0.53 to − 4.38); the model without temporal variables instead directly included that distinction (t = − 8.19, $p < 0.001$; Table S2).

Original TCH systematically underestimated field-measured dominant height. Harmonization corrected this bias while preserving measurement uncertainty (Fig. 3). Models performed similarly with and without temporal variables: respectively, systematic bias decreased from 2.53 (± 2.06) m to 0.01 (± 1.80) m and 0.01 (± 1.79) m, RMSE decreased from 3.27 m to 1.80 m and 1.79 m (47% reduction), and R^2 improved from 0.73 to 0.92 in both. Year-specific (Table S3) and species-specific (Table S4) results confirmed consistent harmonization across strata. Given their similar performance, we adopted the model without temporal variables for subsequent analyses.

3.2. Species-specific reference trajectories of vertical growth

Across the 500 plots sampled per species, harmonization increased initial TCH and reduced estimated vertical growth trends by 6% compared to the original data (from 0.36 (± 0.24) to 0.34 (± 0.24) m/yr; Wilcoxon test, p-value < 0.001).

In the species-specific reference trajectories modeled from these samples, vertical growth decreased as the initial height increased, with declines at lower initial TCH for plots dominated by broadleaves rather than conifers (Fig. 4), all of the latter declining more gradually as indicated by their higher decay coefficients (Kb; 0.94 − 0.98 vs 0.92 − 0.93). Vertical growth trend at minimal height (Ka) was more heterogeneous among conifer trajectories (0.76–1.01) than broadleaves (1.01–1.13). Harmonization increased K_a for all species but Douglas-fir, whereas K_b remained nearly unchanged, indicating a shift in the curves' initial magnitude rather than their shapes.

3.3. Vertical growth patterns

Across all three sites, both vertical growth trends (Fig. 5d) and deviations from reference trajectories (Fig. 5e) demonstrated significant spatial clustering over 2006–2021 (Table 4), with Moran's I of 0.37–0.55 for growth and 0.31–0.46 for deviation (all $p < 0.001$).

In Site A, most cells showed positive growth over 2006–2021 (Fig. 5d), with higher values for coniferous species (spruce and Douglas-fir; Fig. 5b), more pronounced at lower initial TCH (Fig. 5c). Negative growth mainly occurred in disturbed coniferous cells, whereas most broadleaf cells exhibited consistent growth, particularly stable for taller stands (Fig. 5c).

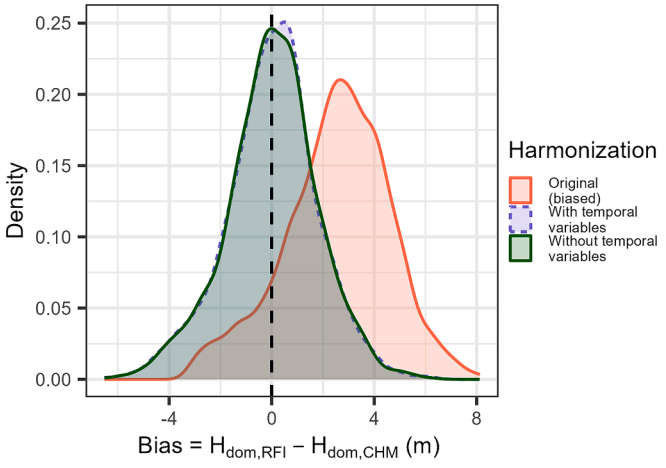

Fig. 3. Distribution of dominant height bias before and after harmonization, using both model versions. Dashed line indicates zero bias.

Although cells generally outperformed regional expectations (Fig. 5f), contrasting deviation patterns emerged across Site A (Fig. 5e). Taller, temporally stable beech cells in the center showed negative-leaning deviation, indicating that this stability occurred at lower initial TCH than expected for the region; conversely, most of the other, smaller beech-dominated areas displayed positive deviations. Spruce cells in the east all deviated positively from their reference trajectory, albeit less intensively when initial TCH increased. Similarly, the heterogeneously composed cells in the west showed better growth than expected for their initial TCH.

To illustrate how deviation patterns vary for the same species across different landscapes, we focused on beech-dominated cells in our three case study sites (Fig. 6). Whereas Site A's beech displayed evenly distributed deviations, Site B's were mostly negative, while Site C exhibited the greatest within-site variability, containing both over- and under-performing beech cells. Propagation of harmonization uncertainty through both growth trends (Eq. (3) and initial heights (Eq. (4) yielded a noise-to-signal ratio equal to 3% of typical deviation magnitude.

4. Discussion

Our workflow derived spatially explicit patterns of canopy height dynamics from harmonized multi-source time series of dominant height. Growth consistently decreased as initial TCH increased, describing realistic species-specific trajectories. Deviations from these reference trajectories displayed spatially clustered patterns different from absolute vertical growth in otherwise similar stands, indicating systematic variations in forest performance. Relying on commonly available data in forested regions, this approach offers multi-scale transferability for remote sensing-based forest monitoring.

4.1. Systematic bias harmonization

Harmonizing TCH against field-based dominant height with consistent measurement protocols successfully reduced systematic bias, providing multi-source time series that describe genuine canopy dynamics rather than acquisition-related artifacts (Wulder et al., 2008). Similarly to Michez et al. (2020), acquisition year was the only temporal variable selected but did not substantially improve TCH estimation (similar RMSE and R^2, unchanged bias; Fig. 3), likely because all acquisitions were conducted during leaf-on season with minimal foliar alteration of canopy structure. Lidar CHMs systematically delivered smaller biases than DAP (Table S3), consistent with previous comparisons (Mielcarek et al., 2020). Retaining the source distinction in the model without temporal variables captured most variance otherwise attributable to acquisition year (Table S2), further supporting CHM source over acquisition timing as the more robust and parsimonious harmonization approach, while identical structural predictors in both versions confirmed that canopy structure primarily drives TCH bias. Beyond canopy heterogeneity and gap fraction known to be smoothed in DSMs (St-Onge et al., 2008), the broadleaf-to-conifer ratio had the most explanatory power, reflecting variations in crown geometry: coniferous-dominated plots displayed larger dominant height biases, their treetops being more difficult to capture (Table S4; Korpela, 2004).

Systematically distributed field plots allowed harmonization over larger extents than point-cloud alignment methods, yielding regional transferability without sacrificing performance. The 6% reduction of vertical growth that we observed after harmonization contrasted with the 37% increase reported by Riofrío et al. (2022), though with ALS-only acquisitions. In our reference trajectories however, harmonization increased vertical growth trend at minimal initial TCH (K_a) but left the curves' shape (K_b) essentially unchanged, indicating that systematic bias in dominant height estimates did not alter growth patterns themselves. Beyond the regional scale of our study likely attenuating local

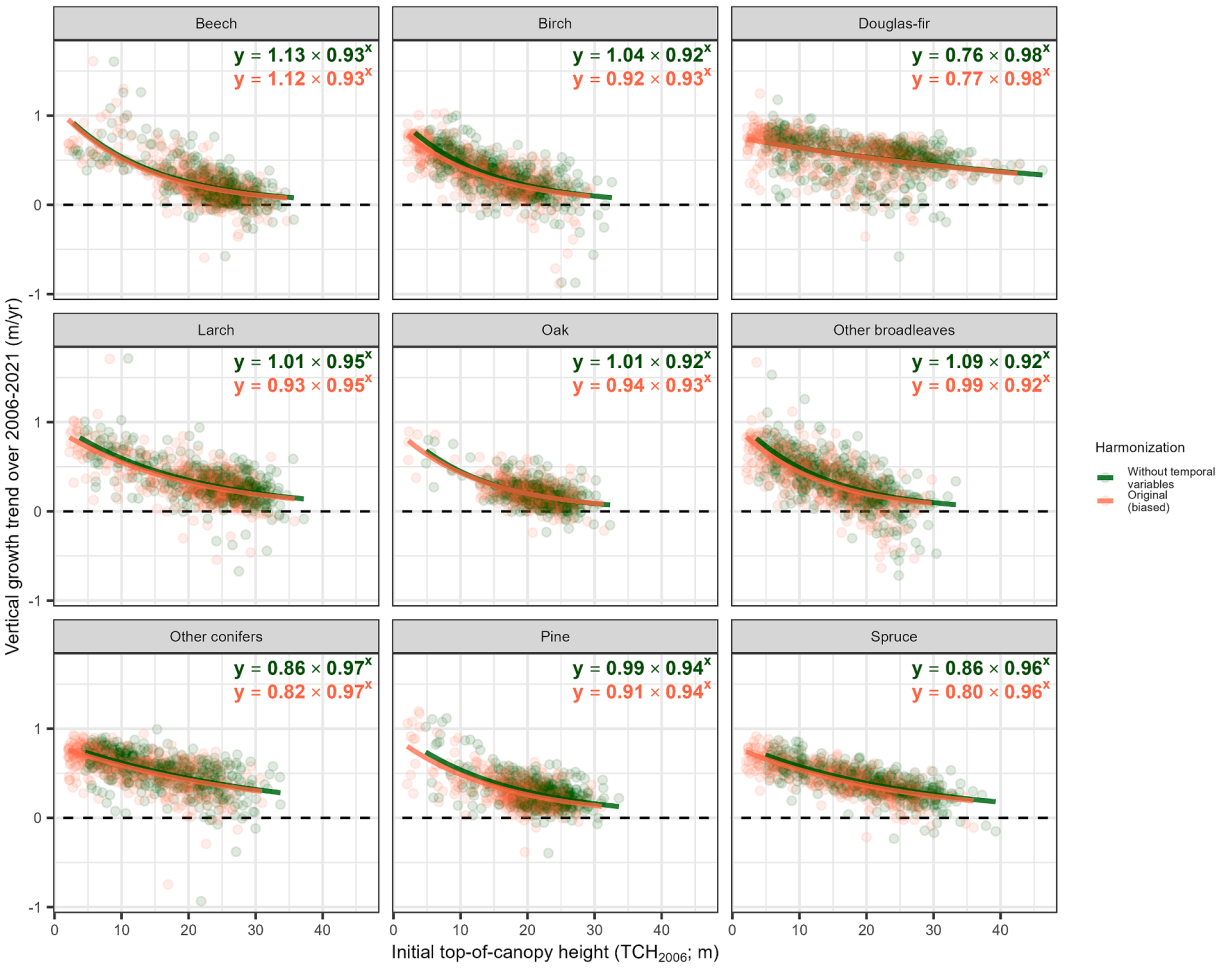

Fig. 4. Reference growth trajectories per species, before and after bias harmonization. Exponential decay models (Eq. (4) fitted per species on 500 random plots, where K_a is vertical growth at minimal initial TCH and K_b the decay coefficient. All NLS models converged (p-value < 0.001).

discrepancies, these limited effects both reflected the comparability of our canopy height products despite differing sources, and our use of multi-year modeling (Eq. (3) rather than pairwise differences to estimate growth (Hopkinson et al., 2008; Coops, 2015). Propagated harmonization uncertainty (Eqs. 3–4) accounted for only 3% of typical deviation magnitude, confirming again that performance patterns reflected genuine variations beyond harmonization artifacts. Still, we recommend harmonization to ensure inter-compatibility when fusing multiple sources of canopy height (Goodbody et al., 2017), and especially advise including temporal variables when transferring the approach to deciduous forests, where phenological differences across seasons may trigger additional bias (St-Onge et al., 2008).

4.2. *Detection of ecologically realistic vertical growth patterns*

We captured ecologically plausible patterns of vertical growth, supporting the feasibility of fine-scale, spatially explicit monitoring of canopy height dynamics from multi-source time series. By relying on space-for-time substitution with initial TCH as a development-stage proxy, as in Riofrío et al. (2023) and Schwartz et al. (2025), we obtained biologically realistic vertical growth estimates over our 15-year period: most fell below 1 m/yr, in line with actual field-reported observations (Perin et al., 2013; Kazimirović et al., 2026) and remotely sensed estimates across temperate forests (Senécal et al., 2018; Dalponte et al., 2019). Because RFI plots were single-visit, our growth trends could only be assessed indirectly, through the plausibility of the reference trajectories rather than against repeated field measurements.

As for these reference trajectories, the exponential-decay formulation adequately captured how vertical growth saturates with developmental stage (Pretzsch, 2020). Lower K_b in broadleaves reflected typically earlier declines than conifers (Fig. 4), which sustained growth until higher heights as already observed by Perin et al. (2013) in the Ardenne. We emphasize that these trajectories depend inherently on regional context, assuming broadly similar site conditions and management histories across sampled plots; they also depend on the composition map's accuracy, since misclassification would distort the species-specific trajectory itself. Yet, they remain indicative of varying species-level development strategies (Dalponte et al., 2019).

The case study revealed that, despite homogeneous and spatially clustered vertical growth patterns between adjacent forest cells of similar composition at Site A (Fig. 5b and 5d, Table 4), deviations distinguished different patterns of performance (Fig. 5e and 5f). Mapping these variations reveals small-scale processes beyond those captured by initial TCH and dominant species alone (Fig. 5b and 5c), consistent with evidence that growth locally varies with both structural and demographic heterogeneity (Begović et al., 2026). Deviation clusters could therefore pinpoint areas of intense competition, previously shown to influence growth in European stands (Vannoppen et al., 2019; Jacobs et al., 2021; Tymińska-Czabańska et al., 2022), or reactions to silvicultural interventions, besides thinning to which dominant height shows limited sensitivity (Weiskittel et al., 2011). Our cross-site, beech-focused comparison of deviations reinforced this diagnostic capability (Fig. 6): balanced deviations at well-drained Site A suggested generally better growth conditions than both other sites, which displayed negative

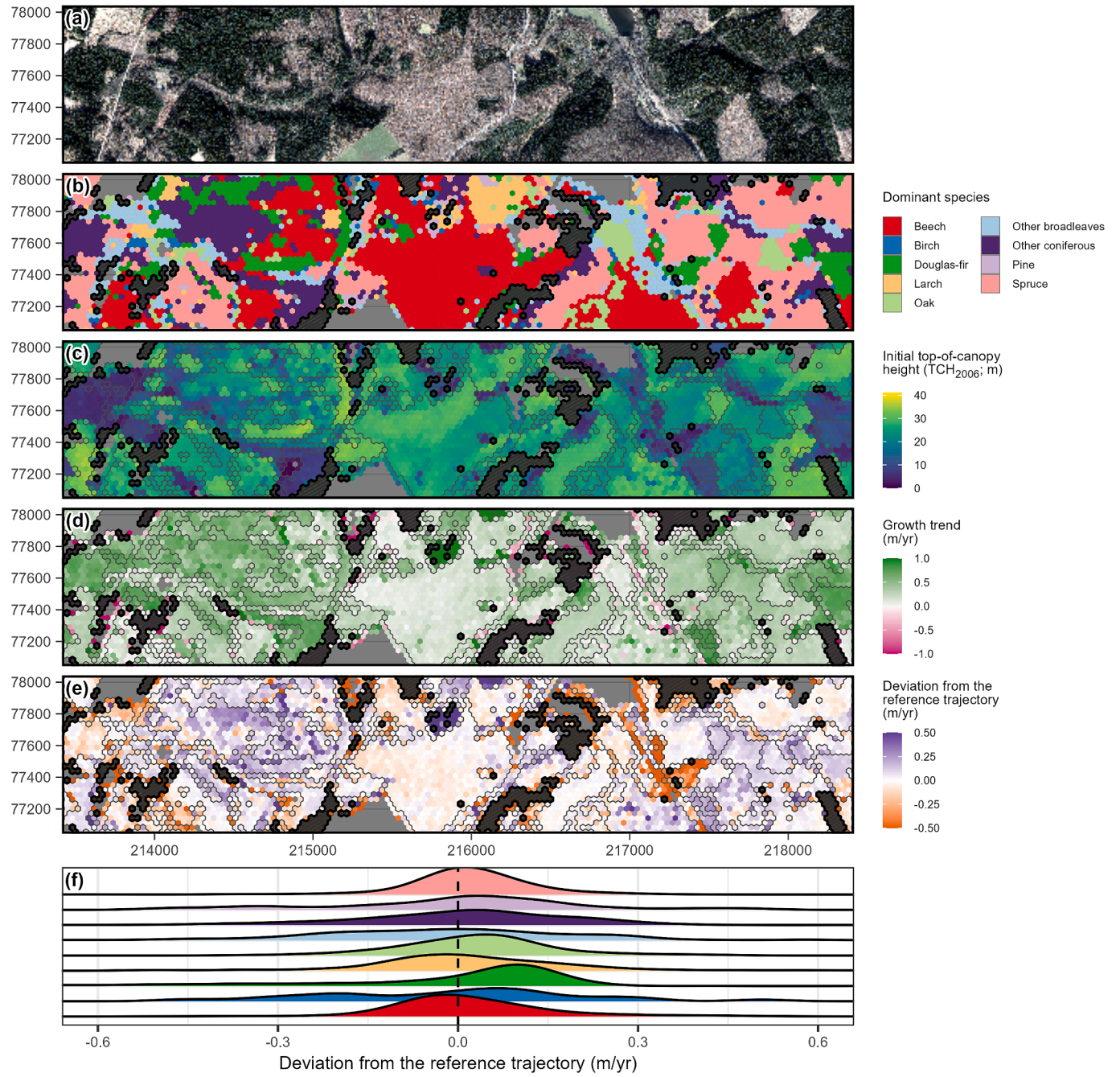

Fig. 5. Vertical growth and deviation from reference trajectory for Site A in the Ardenne, Belgium, at ~ 1000 m² forest cells. (a) recent leaf-off aerial orthophotograph; (b) dominant species; (c) initial top-of-canopy height (2006); (d) vertical growth trend for 2006–2021 and (e) deviation from species-specific expected growth. Panel (f) shows the site-specific distribution of deviation per species, colored as in (b). Disturbed cells (§2.4.1) are greyed out in (b)–(e) to avoid misinterpretation, as they consistently exhibit negative deviations. Coordinates in EPSG:31370 (m).

Table 4
Spatial autocorrelation of vertical growth and deviation patterns. Moran's I for cell-level growth trends and deviations over 2006–2021 across the three case study sites.

Site	Growth	Deviation
A	0.55 ($p < 0.001$)	0.34 ($p < 0.001$)
B	0.55 ($p < 0.001$)	0.46 ($p < 0.001$)
C	0.37 ($p < 0.001$)	0.31 ($p < 0.001$)

and more contrasted deviation patterns, in line with Aertsen et al. (2014) who demonstrated that favorable sites maintained better productivity even under stress. Given beech's ecological plasticity and climate sensitivity (Martinez del Castillo et al., 2022), such site-level microclimatic differences could also modulate the exposure to late frost, waterlogging or droughts induced by climate change (Latte et al., 2016; Zellweger et al., 2020).

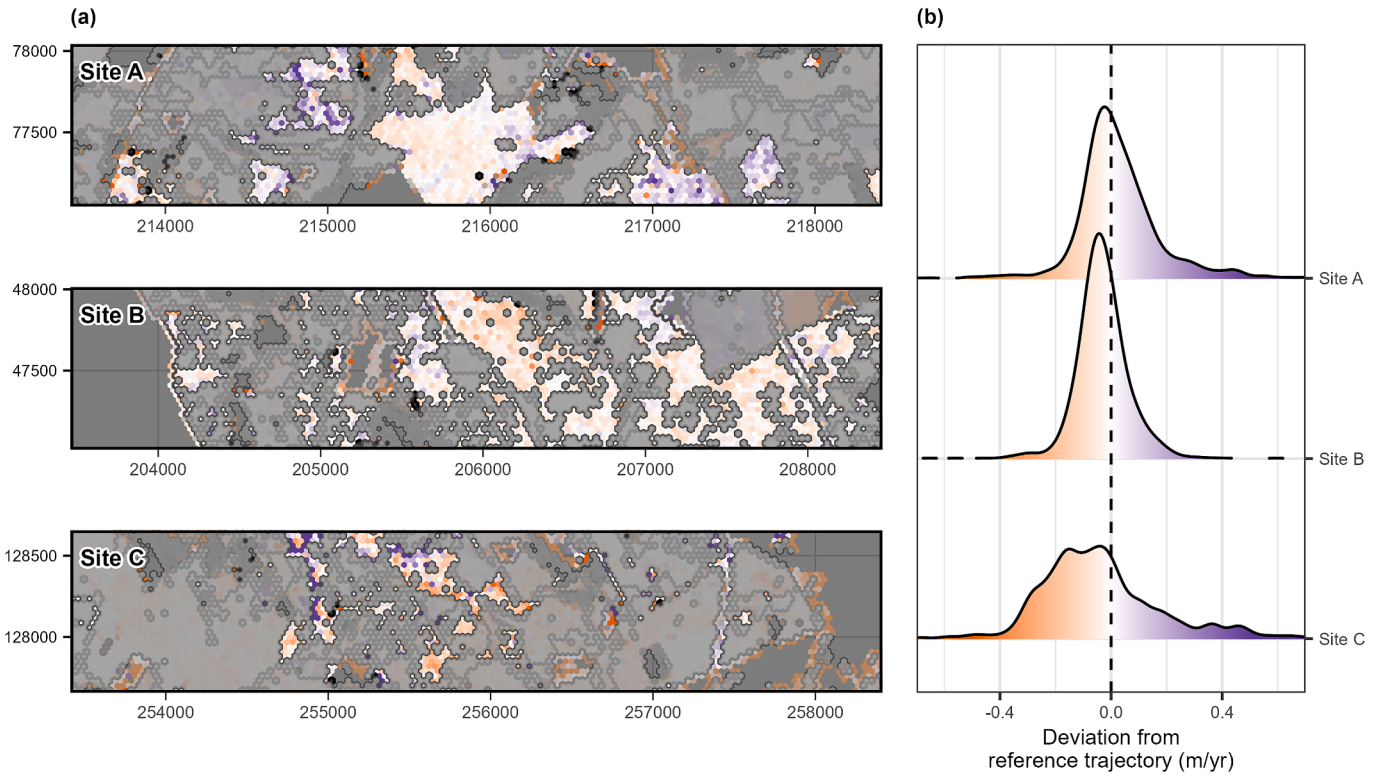

Fig. 6. Beech deviation across sites (5 x 1 km). (a) Spatial distribution of deviation from their reference growth trajectory for beech-dominated cells across three 5 × 1 km^2 sites (A, B, C top to bottom). (b) Beech deviation distribution revealing site-specific patterns, from negative (orange) to positive (purple) deviation; dashed vertical line marks zero deviation from the regional expectation. Coordinates in EPSG:31370 (m). (For interpretation of the references to colour in this figure legend, the reader is referred to the web version of this article.)

4.3. *Transferability and future applications*

Practically, our framework ensures inter-compatibility among heterogeneous datasets. Illustrated here with aerial CHMs routinely acquired for other purposes, this straightforward approach may prove particularly valuable for fusing multi-source air- and, potentially, spaceborne data towards fine-scale ecological monitoring (Ecke et al., 2022) with potential near real-time applications (Coops et al., 2023). Although the growing availability of wall-to-wall canopy height products (Lang et al., 2023; Tolan et al., 2024; Schwartz et al., 2024) alongside standardized field inventories (Tomppo et al., 2010) could opportunistically densify time series, harmonizing satellite products such as GEDI (Dubayah et al., 2020) remains uncertain as inherently different sampling designs and accuracies would require re-evaluating systematic bias predictors (Moudrý et al., 2026). Satellite-derived growth signals still require aggregation to several kilometers (Schwartz et al., 2025), far coarser than the ~ 1000 m^2 cells resolved here (Fig. 5). Regardless of platform or sensor type, multi-source harmonization requires at least two canopy height products acquired at reasonable intervals to exceed measurement uncertainty (Coops, 2015; Price et al., 2020), and temporally matched field plots as a common reference to ensure time series consistency (Wulder et al., 2008).

Reference trajectories may therefore be generated from local to global scales and stratified by species, functional types, or management contexts depending on data availability, encouraging targeted canopy dynamics monitoring and comparisons. By adding the vertical dimension, structural information resolves a wider range of post-disturbance responses than spectral indices alone (Huettermann et al., 2023), suggesting that resulting deviations could reinforce remote sensing-based resilience assessments, complementing established indicators of ecosystem functioning such as phenology or water content (De Keersmaecker et al., 2015; Runge et al., 2025). We recommend investigating how these deviations can clarify the impacts of external forcings, be they climate events, pest outbreaks, or management interventions (Janiec et al., 2024; Pretzsch, 2020), and whether observed patterns mirror resilience indicators following disturbances (Senf and Seidl, 2021).

5. Conclusion

Harmonized multi-source time series of dominant height reliably characterized vertical dynamics across forests. Deviations from reference trajectories revealed spatially clustered performance contrasts among otherwise similar forests, more exhaustively than field inventory networks. Considering the increasing availability of multi-scale canopy height products, these results demonstrate that repurposed air- and spaceborne datasets can add structural understanding into forest monitoring, complementing spectral and cover-based approaches that currently dominate large-scale assessments. By contextualizing growth into a spatially explicit diagnostic indicator of unusual patterns within forests, this transferable workflow supports evidence-based guidance for targeted and adaptive management (Messier et al., 2015; Fassnacht et al., 2025). We encourage future research to move beyond characterization into investigating which forcings, spatial configurations, or forest attributes drive the deviations and how they interact.

Data and Code availability

Code is available at https://github.com/Hdkam/CHM-growth-dynamics. Canopy height and ancillary rasters are publicly accessible at https://forestimator.gembloux.ulg.ac.be/. Forest inventory data is accessible upon request from the IPRFW (https://iprfw.spw.wallonie.be/).

CRediT authorship contribution statement

Hugo de Lame: Writing – original draft, Visualization, Methodology, Investigation, Formal analysis, Data curation, Conceptualization. **Thibauld Collet:** Writing – review & editing. **Pauline Depoortere:** . **Alexia Favaro:** Writing – review & editing. **Philippe Lejeune:** Writing – review & editing, Resources, Data curation. **Adrien Michez:** Writing – review & editing. **Antoine Plumacker:** Writing – review & editing, Formal analysis, Conceptualization. **Jérôme Perin:** Writing – review & editing, Resources. **Thomas Pollet:** Writing – review & editing. **Quentin Ponette:** Writing – review & editing. **Zoé Rousseau:** Writing – review & editing. **Arthur Vander Linden:** Writing – review & editing, Conceptualization. **Marie-Pierre Tasseroul:** Writing – review & editing. **Christian Messier:** Writing – review & editing, Supervision, Conceptualization. **Jean-François Bastin:** Writing – original draft, Supervision, Conceptualization.

Declaration of competing interest

The authors declare the following financial interests/personal relationships which may be considered as potential competing interests: Hugo de LAME reports financial support was provided by Fund for Research and Training in Industry and Agriculture. If there are other authors, they declare that they have no known competing financial interests or personal relationships that could have appeared to influence the work reported in this paper.

Acknowledgements

This work was supported by the Fund for Research Training in Industry and Agriculture (FRIA, F.R.S-F.N.R.S) and by the Natural Sciences and Engineering Research Council (NSERC) of Canada Alliance through the DIVERSE project. J.-F.B. acknowledges funding support from the Francqui foundation in Belgium, from BELSPO through the Stereo IV AFRO-CARDS (SR/00/410) and Biodiversa+ CoForFunc (RT/24/CoForFunc) projects, and from FNRS EOS call through the CANOPi project (O.0026.22). The authors thank the Inventaire Permanent des Ressources Forestières de Wallonie (IPRFW) for providing access to inventory data.

Appendix A. Supplementary data

Supplementary data to this article detailed harmonization performance and TCH's sensitivity analysis can both be found online at https://doi.org/10.1016/j.jag.2026.105570.

Data availability

A data statement is included in the paper, as some of it is publically accessible while other products must be requested.

References

Aertsen, W., Janssen, E., Kint, V., et al., 2014. Long-term growth changes of common beech (*Fagus sylvatica* L.) are less pronounced on highly productive sites. For. Ecol. Manage. 312, 252–259. https://doi.org/10.1016/j.foreco.2013.09.034.

Alderweireld, M., Burnay, F., Pitchugin, M., et al., 2015. Inventaire Forestier Wallon – Résultats 1994–2012. Service Public de Wallonie, Namur.

Begović, K., Pavlin, J., Langbehn, T., et al., 2026. Demographic and structural variability modulate growth dynamics in European beech primary forests. Glob. Chang. Biol. 32, e70902. https://doi.org/10.1111/gcb.70902.

Bivand, R.S., Pebesma, E., Gómez-Rubio, V., 2013. Applied Spatial Data Analysis with R. Springer, New York. https://doi.org/10.1007/978-1-4614-7618-4.

Bolton, D.K., White, J.C., Wulder, M.A., et al., 2018. Updating stand-level forest inventories using airborne laser scanning and Landsat time series data. Int. J. Appl. Earth Obs. Geoinf. 66, 174–183. https://doi.org/10.1016/j.jag.2017.11.016.

Bolyn, C., Lejeune, P., Michez, A., et al., 2022. Mapping tree species proportions from satellite imagery using spectral–spatial deep learning. Remote Sens. Environ. 280, 113205. https://doi.org/10.1016/j.rse.2022.113205.

Coops, N.C., 2015. Characterizing forest growth and productivity using remotely sensed data. Curr. For. Rep. 1, 195–205. https://doi.org/10.1007/s40725-015-0020-x.

Coops, N.C., Tompalski, P., Goodbody, T.R.H., et al., 2023. Framework for near real-time forest inventory using multi source remote sensing data. for.: Int. J. For. Res. 96, 1–19. https://doi.org/10.1093/forestry/cpac015.

Dalponte, M., Jucker, T., Liu, S., et al., 2019. Characterizing forest carbon dynamics using multi-temporal lidar data. Remote Sens. Environ. 224, 412–420. https://doi.org/10.1016/j.rse.2019.02.018.

De Keersmaecker, W., Lhermitte, S., Tits, L., et al., 2015. A model quantifying global vegetation resistance and resilience to short-term climate anomalies and their relationship with vegetation cover. Glob. Ecol. Biogeogr. 24, 539–548. https://doi.org/10.1111/geb.12279.

Dubayah, R., Blair, J.B., Goetz, S., et al., 2020. The global ecosystem dynamics investigation: high-resolution laser ranging of the Earth's forests and topography. Sci. Remote Sens. 1, 100002. https://doi.org/10.1016/j.srs.2020.100002.

Ecke, S., Dempewolf, J., Frey, J., et al., 2022. UAV-based forest health monitoring: a systematic review. Remote Sens. 14, 3205. https://doi.org/10.3390/rs14133205.

Ehbrecht, M., Seidel, D., Annighöfer, P., et al., 2021. Global patterns and climatic controls of forest structural complexity. Nat. Commun. 12, 519. https://doi.org/10.1038/s41467-020-20767-z.

Falk, D.A., Van Mantgem, P.J., Keeley, J.E., et al., 2022. Mechanisms of forest resilience. For. Ecol. Manage. 512, 120129. https://doi.org/10.1016/j.foreco.2022.120129.

Fassnacht, F.E., Mager, C., Waser, L.T., et al., 2025. Forest practitioners' requirements for remote sensing-based canopy height, wood-volume, tree species, and disturbance products. for.: Int. J. For. Res. 98, 233–252. https://doi.org/10.1093/forestry/cpae021.

Feng, Y., Su, H., Tang, Z., et al., 2021. Reduced resilience of terrestrial ecosystems locally is not reflected on a global scale. Commun. Earth Environ. 2, 88. https://doi.org/10.1038/s43247-021-00163-1.

Gilles, A., Jonathan, L., Juliette, C., et al., 2024. Spatial and remote sensing monitoring shows the end of the bark beetle outbreak on Belgian and north-eastern France Norway spruce (*Picea abies*) stands. Environ. Monit. Assess. 196, 226. https://doi.org/10.1007/s10661-024-12372-0.

Goodbody, T.R.H., Coops, N.C., Tompalski, P., et al., 2017. Updating residual stem volume estimates using ALS- and UAV-acquired stereo-photogrammetric point clouds. Int. J. Remote Sens. 38, 2938–2953. https://doi.org/10.1080/01431161.2016.1219425.

Goodbody, T.R.H., Coops, N.C., White, J.C., 2019. Digital aerial photogrammetry for updating area-based forest inventories: a review of opportunities, challenges, and future directions. Curr. For. Rep. 5, 55–75. https://doi.org/10.1007/s40725-019-00087-2.

Hansen, M.C., Potapov, P.V., Moore, R., et al., 2013. High-resolution global maps of 21st-century forest cover change. Science 342, 850–853. https://doi.org/10.1126/science.1244693.

Hopkinson, C., Chasmer, L., Hall, R.J., 2008. The uncertainty in conifer plantation growth prediction from multi-temporal lidar datasets. Remote Sens. Environ. 112, 1168–1180. https://doi.org/10.1016/j.rse.2007.07.020.

Huettermann, S., Jones, S., Soto-Berelov, M., et al., 2023. Using Landsat time series and bi-temporal GEDI to compare spectral and structural vegetation responses after fire. Int. J. Appl. Earth Obs. Geoinf. 122, 103403. https://doi.org/10.1016/j.jag.2023.103403.

Hyyppä, J., Yu, X., Rönnholm, P., et al., 2003. Factors affecting object-oriented forest growth estimates obtained using laser scanning. Photogramm. J. Finl. 18, 16–31.

Jacobs, K., Bonal, D., Collet, C., et al., 2021. Mixing increases drought exposure through a faster growth in beech, but not in oak. For. Ecol. Manage. 479, 118593. https://doi.org/10.1016/j.foreco.2020.118593.

Janiec, P., Hawryło, P., Tymińska-Czabańska, L., et al., 2024. Digital aerial photogrammetry as a spatial and temporal extension of ALS in forest height growth modeling. Int. J. Digit. Earth 17, 2418879. https://doi.org/10.1080/17538947.2024.2418879.

Kazimirović, M., Stajić, B., Petrović, N., et al., 2026. New site index models unravel: European beech (*Fagus sylvatica* L.) sustains high productivity in western Serbia's dry continental climate. for.: Int. J. For. Res. 99, cpag025. https://doi.org/10.1093/forestry/cpag025.

Korpela, I., 2004. Individual tree measurements by means of digital aerial photogrammetry. Silva Fenn. Monogr. 3, 1–94. https://doi.org/10.14214/sf.sfm3.

Lang, N., Jetz, W., Schindler, K., et al., 2023. A high-resolution canopy height model of the Earth. Nat. Ecol. Evol. 7, 1778–1789. https://doi.org/10.1038/s41559-023-02206-6.

Latte, N., Perin, J., Kint, V., et al., 2016. Major changes in growth rate and growth variability of beech (*Fagus sylvatica* L.) related to soil alteration and climate change in Belgium. Forests 7, 174. https://doi.org/10.3390/f7080174.

Leclère, L., Latte, N., Candaele, R., et al., 2024. Estimation of within-gap regeneration height growth in managed temperate deciduous forests using bi-temporal airborne laser scanning data. Ann. For. Sci. 81, 36. https://doi.org/10.1186/s13595-024-01252-9.

Lejeune, P., Latte, N., Perin, J., et al., 2025. De nouvelles couches cartographiques pour mieux décrire la forêt wallonne. For. Nat. 175, 1–13.

Markus, T., Neumann, T., Martino, A., et al., 2017. The ice, cloud, and land elevation satellite-2 (ICESat-2): science requirements, concept, and implementation. Remote Sens. Environ. 190, 260–273. https://doi.org/10.1016/j.rse.2016.12.029.

Martinez del Castillo, E., Zang, C.S., Buras, A., et al., 2022. Climate-change-driven growth decline of European beech forests. Commun. Biol. 5, 163. https://doi.org/10.1038/s42003-022-03107-3.

McRoberts, R.E., Næsset, E., Gobakken, T., et al., 2015. Indirect and direct estimation of forest biomass change using forest inventory and airborne laser scanning data. Remote Sens. Environ. 164, 36–42. https://doi.org/10.1016/j.rse.2015.02.018.
Messier, C., Puettmann, K., Chazdon, R., et al., 2015. From management to stewardship: viewing forests as complex adaptive systems in an uncertain world. Conserv. Lett. 8, 368–377. https://doi.org/10.1111/conl.12156.
Michez, A., Huylenbroeck, L., Bolyn, C., et al., 2020. Can regional aerial images from orthophoto surveys produce high quality photogrammetric canopy height model? a single tree approach in western Europe. Int. J. Appl. Earth Obs. Geoinf. 92, 102190. https://doi.org/10.1016/j.jag.2020.102190.
Mielcarek, M., Kamińska, A., Stereńczak, K., 2020. Digital aerial photogrammetry (DAP) and airborne laser scanning (ALS) as sources of information about tree height: comparisons of the accuracy of remote sensing methods for tree height estimation. Remote Sens. 12, 1808. https://doi.org/10.3390/rs12111808.
Moudrý, V., Remelgado, R., Forkel, M., et al., 2026. Spaceborne canopy height products should be complemented with airborne laser scanning data: toward a European canopy height model. Earth Space Sci. 13, e2025EA004544. https://doi.org/10.1029/2025EA004544.
Næsset, E., 2002. Predicting forest stand characteristics with airborne scanning laser using a practical two-stage procedure and field data. Remote Sens. Environ. 80, 88–99. https://doi.org/10.1016/S0034-4257(01)00290-5.
Oliver, C.D., Larson, B.C., 1996. Forest Stand Dynamics, updated ed. Wiley, New York.
Perin, J., 2023. Tree species composition, structure and localisation measured in the permanent sample plots of the Walloon forest inventory between 2014 and 2020. Service Public de Wallonie (SPW-ARNE), Inventaire Permanent des Ressources Forestières de Wallonie. https://environnement.wallonie.be/home/milieux/forets-et-nature/forets-wallonnes/en-chiffres-et-en-cartes.html (accessed 1 September 2026).
Perin, J., Hébert, J., Brostaux, Y., et al., 2013. Modelling the top-height growth and site index of Norway spruce in southern Belgium. For. Ecol. Manage. 298, 62–70. https://doi.org/10.1016/j.foreco.2013.03.009.
Pretzsch, H., 2020. The course of tree growth. Theory and Reality. for. Ecol. Manage. 478, 118508. https://doi.org/10.1016/j.foreco.2020.118508.
Pretzsch, H., Biber, P., Schütze, G., et al., 2014. Forest stand growth dynamics in Central Europe have accelerated since 1870. Nat. Commun. 5, 4967. https://doi.org/10.1038/ncomms5967.
Price, B., Waser, L.T., Wang, Z., et al., 2020. Predicting biomass dynamics at the national extent from digital aerial photogrammetry. Int. J. Appl. Earth Obs. Geoinf. 90, 102116. https://doi.org/10.1016/j.jag.2020.102116.
Riofrío, J., White, J.C., Tompalski, P., et al., 2022. Harmonizing multi-temporal airborne laser scanning point clouds to derive periodic annual height increments in temperate mixedwood forests. Can. J. For. Res. 52, 1334–1352. https://doi.org/10.1139/cjfr-2022-0055.
Riofrío, J., White, J.C., Tompalski, P., et al., 2023. Modelling height growth of temperate mixedwood forests using an age-independent approach and multi-temporal airborne laser scanning data. For. Ecol. Manage. 543, 121137. https://doi.org/10.1016/j.foreco.2023.121137.
Rondeux, J., 2021. La Mesure des Arbres et des Peuplements Forestiers. Uliège Library, Gembloux.
Runge, K., Tucker, M., Crowther, T.W., et al., 2025. Monitoring terrestrial ecosystem resilience using earth observation data: identifying consensus and limitations across metrics. Glob. Chang. Biol. 31, e70115. https://doi.org/10.1111/gcb.70115.
Schlund, M., Magdon, P., Eaton, B., et al., 2019. Canopy height estimation with TanDEM-X in temperate and boreal forests. Int. J. Appl. Earth Obs. Geoinf. 82, 101904. https://doi.org/10.1016/j.jag.2019.101904.
Schwartz, M., Ciais, P., Ottlé, C., et al., 2024. High-resolution canopy height map in the Landes forest (France) based on GEDI, Sentinel-1, and Sentinel-2 data with a deep learning approach. Int. J. Appl. Earth Obs. Geoinf. 128, 103711. https://doi.org/10.1016/j.jag.2024.103711.
Schwartz, M., Ciais, P., Sean, E., et al., 2025. Retrieving yearly forest growth from satellite data: a deep learning based approach. Remote Sens. Environ. 330, 114959. https://doi.org/10.1016/j.rse.2025.114959.
Seidl, R., Thom, D., Kautz, M., et al., 2017. Forest disturbances under climate change. Nat. Clim. Chang. 7, 395–402. https://doi.org/10.1038/nclimate3303.
Senécal, J.-F., Doyon, F., Messier, C., 2018. Disentangling the causes of canopy height increase in managed and unmanaged temperate deciduous forests using multi-temporal airborne laser scanning. Remote Sens. Environ. 217, 233–243. https://doi.org/10.1016/j.rse.2018.08.023.
Senf, C., Seidl, R., 2021. Mapping the forest disturbance regimes of Europe. Nat. Sustain. 4, 63–70. https://doi.org/10.1038/s41893-020-00609-y.
St-Onge, B., Vega, C., Fournier, R.A., et al., 2008. Mapping canopy height using a combination of digital stereo-photogrammetry and lidar. Int. J. Remote Sens. 29, 3343–3364. https://doi.org/10.1080/01431160701469040.
Tolan, J., Yang, H.-I., Nosarzewski, B., et al., 2024. Very high resolution canopy height maps from RGB imagery using self-supervised vision transformer and convolutional decoder trained on aerial lidar. Remote Sens. Environ. 300, 113888. https://doi.org/10.1016/j.rse.2023.113888.
Tomppo, E., Gschwantner, T., Lawrence, M., et al. (Eds.), 2010. National Forest Inventories: Pathways for Common Reporting. Springer, Dordrecht. Doi: 10.1007/978-90-481-3233-1.
Tossens, S., Lisein, J., Cordier, S., et al., 2024. Guide des Stations Forestières d'Ardenne, Tome 1: L'Ardenne. Ediwal/DNF, Namur.
Tymińska-Czabańska, L., Hawryło, P., Socha, J., 2022. Assessment of the effect of stand density on the height growth of Scots pine using repeated ALS data. Int. J. Appl. Earth Obs. Geoinf. 108, 102763. https://doi.org/10.1016/j.jag.2022.102763.
Valavi, R., Elith, J., Lahoz-Monfort, J.J., et al., 2019. blockCV: an R package for generating spatially or environmentally separated folds for k-fold cross-validation of species distribution models. Methods Ecol. Evol. 10, 225–232. https://doi.org/10.1111/2041-210X.13107.
Vannoppen, A., Kint, V., Ponette, Q., et al., 2019. Tree species diversity impacts average radial growth of beech and oak trees in Belgium, not their long-term growth trend. For. Ecosyst. 6, 10. https://doi.org/10.1186/s40663-019-0169-z.
Weiskittel, A.R., Hann, D.W., Kershaw, J.A., et al., 2011. Forest Growth and Yield Modeling, first ed. Wiley, Chichester. Doi: 10.1002/9781119998518.
Wood, S., 2000. mgcv: mixed GAM computation vehicle with automatic smoothness estimation [software]. CRAN. https://doi.org/10.32614/CRAN.package.mgcv.
Woodcock, C.E., Loveland, T.R., Herold, M., et al., 2020. Transitioning from change detection to monitoring with remote sensing: a paradigm shift. Remote Sens. Environ. 238, 111558. https://doi.org/10.1016/j.rse.2019.111558.
Wu, D., Johansen, K., Phinn, S., et al., 2020. Inter-comparison of remote sensing platforms for height estimation of mango and avocado tree crowns. Int. J. Appl. Earth Obs. Geoinf. 89, 102091. https://doi.org/10.1016/j.jag.2020.102091.
Wulder, M.A., White, J.C., Coops, N.C., et al., 2008. Multi-temporal analysis of high spatial resolution imagery for disturbance monitoring. Remote Sens. Environ. 112, 2729–2740. https://doi.org/10.1016/j.rse.2008.01.010.
Yu, X., Hyyppä, J., Kaartinen, H., et al., 2008. Obtaining plotwise mean height and volume growth in boreal forests using multi-temporal laser surveys and various change detection techniques. Int. J. Remote Sens. 29, 1367–1386. https://doi.org/10.1080/01431160701736356.
Zellweger, F., De Frenne, P., Lenoir, J., et al., 2020. Forest microclimate dynamics drive plant responses to warming. Science 368, 772–775. https://doi.org/10.1126/science.aba6880.
Zhang, B., Jackson, T.D., Coomes, D.A., et al., 2025. Soils and topography drive large and predictable shifts in canopy dynamics across tropical forest landscapes. New Phytol. 247, 1666–1679. https://doi.org/10.1111/nph.70300.